

# Which part of the Brillouin zone contributes most to the high-harmonic radiation?

M. Kolesik

*James Wyant College of Optical Sciences, The University of Arizona, Tucson, AZ 85721, U.S.A.*

Utilizing realistic simulations of high-harmonic generation (HHG) in several materials, we study how different regions of the Brillouin zone contribute to the nonlinear response. It is often assumed that only the vicinity of the  $\Gamma$  point is predominantly responsible for the HHG spectrum, but it is shown here that such an approximation is inaccurate in general. While examples can be identified where merely 0.4% of the Brillouin zone produces semi-quantitatively accurate HHG-spectra, in most situations one must include at least thirty to fifty percent of the Brillouin-zone volume to obtain accurate above-the-gap harmonics. For the harmonic peaks below the bandgap energy, the current-density responses from the entire Brillouin zone must always be integrated. We also identify the minimal set of electronic bands necessary for the construction of reduced but still realistic HHG-models. The results should be useful for a number of HHG applications, including all-optical reconstructions of the band-structure and light-matter couplings, or considerations involving semi-classical approaches to solid-state high-harmonic radiation.

## I. INTRODUCTION

Ever since the first observations of the above-the-gap harmonic generation from a solid-state medium [1], numerous efforts continue [2] to understand the underlying physics, and to utilize this extremely nonlinear effect [3, 4] for applications opening new windows into the quantum world of materials. The solid-state high-harmonic generation (HHG) has emerged as a tool to map the band-structures of materials and to investigate their dynamics with an unprecedented resolution. However, harnessing its full potential as a probe will require detailed understanding of the contributions from different electronic states. In particular, it is necessary to quantify how different parts of the Brillouin zone contribute to the HHG-signal, and which bands take part in the dynamics.

The question of “where in the Brillouin zone is the source” of the high-harmonic signal, underlines not only some HHG interpretations but also a number of applications, including all-optical reconstruction of the electronic band-structure [5–7], characterization of light-matter couplings [8–12], and probing the topological properties of materials [13–16]. Here, the notion of trajectory, be it in real or reciprocal space, often plays a role.

Originally inspired by the success of the strong-field approximation in the HHG from atoms, the three-step model [17–19], its variations [6, 20, 21] and generalizations [22] were adopted to the solid-state context [23]. A common feature among the strong-field and semi-classical approaches is that there is an “excitation step” when tunneling from the valence to the conduction band occurs at or close to the  $\Gamma$ -point (or at the location of the minimal energy gap). While it has been pointed out [24] that the minimal-gap location does not necessarily dominate the whole HHG process, the assumptions that the interband excitation peaks sharply around the point of minimal gap are rarely tested in concrete situations (however, see [16] for a notable exception).

The importance of electronic trajectories and their manifestations in the nonlinear response of materials is one of the motivations for this work. However, beyond the strong-field and semi-classical approaches, quantitative mapping of the Brillouin zone and of the various contributions to the solid-state HHG is conceptually important in its own right, and it is our main goal. This work concentrates on three-dimensional materials, and utilizes realistic numerical simulations to compare how different regions of the Brillouin zone shape the high-harmonic responses.

Our results will show that there is a qualitative difference between the behaviors of the below-gap and the above-gap harmonics. While for the lower-order harmonic radiation the contributions from the entire Brillouin zone are always necessary to achieve quantitatively accurate description, only thirty to fifty percent of the Brillouin zone volume is sufficient to capture a great majority of the higher-order harmonic radiation. However, it turns out that, at least for the three-dimensional materials, the assumption that the electronic states from around the  $\Gamma$  point contribute the most of the HHG response is unrealistic in general.

Such a finding may seem to contradict the fact that the tunneling is by far most likely where the energy gap is minimal. To clarify this issue, we investigate what portion of the excited carriers are actually “born” in the central part of the Brillouin zone. It will be shown that despite the local tunneling rate being much larger around  $\Gamma$ , the rest of the zone still generates the great majority of the excited carriers. Their collective response to the driving field therefore cannot be always neglected.

We also address the question concerning the minimal set of electronic bands that should be included in a reduced model. While some spectral features can be obtained already with a few bands, accurate results require inclusion of bands in sets that are “connected” via degenerate points or via avoided band crossings.

## II. MATERIAL MODELS

This work utilizes the empirical tight-binding models for several materials with zinc blende and diamond structures. Most of our simulations were performed for GaAs. Besides the fact that it is an important material, this choice is also motivated by the fact that many experimental results are available for this material (see e.g. [25, 26]). Some of the measurements [26] were previously used to verify the accuracy of the model used in this paper. We have demonstrated that the tight-binding description of GaAs, both with and without spin-orbit coupling, provides the nonlinear optical response which agrees quite well with HHG measurements [27]. It was also shown that the model correctly captures the second-order nonlinearity of the material [28]. In other words, the tight-binding description of GaAs, coupled with the recently introduced HHG simulator [29] has been tested across the frequency range including below-bandgap and above-bandgap harmonics. This gives us confidence to draw conclusions from the numerical simulations.

The next material included in our comparative simulations is CdTe. It was recently identified as a medium in which harmonics up to and beyond order of thirty were generated at a very low excitation intensity [30]. The low-intensity and flux needed for the high-order harmonic generation makes this material very interesting. One reason this medium is suitable for the present purpose is that it complements GaAs. It was argued in Ref. [30] that the special feature that makes CdTe to stand apart is the flatness of its conduction band. The flatness implies a high density of states in the vicinity of the  $\Gamma$ -point, which in turn makes it possible to argue that the center of the Brillouin zone should command the HHG process even more than in GaAs. The strength of the  $\Gamma$ -point contribution is precisely the feature which we aim to investigate.

To broaden our set of material models, we choose crystalline Silicon as a material which differs from GaAs and CdTe in that it is inversion symmetric. The higher material symmetry eliminates even-order harmonic generation, and gives rise to simpler spectra in which it is perhaps easier to investigate which part of the Brillouin zone contributes most. Unlike GaAs, crystalline Silicon does not possess a direct gap. Consequently, it is not straightforward to make an argument for a specific location in the Brillouin zone to be the strongest “source” of high-harmonic radiation. It should be interesting to see if direct- and indirect-gap media behave differently in this respect.

The description of the materials in this work is based on the same, so called  $sp^3s^*$  tight-binding model [31]. It is applicable to both the zinc blende and the diamond structures. As an input for the sgiSBE solver [28, 29] which was used to simulate the HHG spectra, the explicit expressions for the  $\mathbf{k}$ -dependent Hamiltonian  $h(\mathbf{k})$  was obtained from [32]. The parameter sets were taken from [31] for GaAs and Silicon, and from [33] for CdTe. For the results shown in what follows, we applied the

spin-degenerate version of the material models.

## III. NUMERICAL MODELING OF SOLID-STATE HHG

HHG simulations in this work were done with the structure-gauge-independent SBE solver (sgiSBEs). We refer the Reader to the descriptions of the algorithm given in [29] and also in [28], and include a brief summary here. For each  $\mathbf{k}$  sampling the Brillouin zone, the initial density matrix  $\rho_{mn}(\mathbf{k}; t = 0)$  is set to be the zero-temperature density matrix representing full valence and empty conduction bands. One integration step, or an update from time  $t_i$  to time  $t_{i+1}$ , can be written as an operator splitting scheme in the form

$$\rho_{mn}(\mathbf{k}; t_{i+1}) = \sum_{a,b} \langle m\mathbf{k}_{i+1} | a\mathbf{k}_i \rangle \times e^{-i\epsilon_a(\mathbf{k}_i)\Delta} \rho_{ab}(\mathbf{k}; t_i) e^{+i\epsilon_b(\mathbf{k}_i)\Delta} \times \langle b\mathbf{k}_i | n\mathbf{k}_{i+1} \rangle. \quad (1)$$

where  $\Delta = t_{i+1} - t_i$  is the time-step,  $\mathbf{k}_i = \mathbf{k} - \mathbf{A}(t_i)$  with  $\mathbf{A}$  representing the vector potential of the driving pulse, and  $|a\mathbf{k}_i\rangle$  stands for the  $\mathbf{k}$ -dependent Bloch eigenstate in the electronic band  $a$ . The middle row in (1) can be understood as the first split-step which evolves the density matrix in the current Hamiltonian eigenbasis  $\{|a\mathbf{k}_i\rangle\}$ . For the next split-step, the new-time eigenbasis  $\{|b\mathbf{k}_{i+1}\rangle\}$  is obtained by the exact diagonalization of the Hamiltonian  $h(\mathbf{k}_{i+1})$ , and then the density matrix is transformed into the new basis as shown in the first and third rows of (1). This update scheme is applied in parallel, independently for all  $\mathbf{k}$  sampling the Brillouin zone. Dephasing is approximated as usual, in a separate split-step,

$$\rho_{mn}(\mathbf{k}; t) \leftarrow \rho_{mn}(\mathbf{k}; t) \exp[-\Delta t/T_2], \quad (2)$$

with  $T_2$  being the dephasing time, which we set equal to 5 fs, and note that the observations we arrive at in this work are independent of its precise value.

The total observed current density is calculated as an integral over the complete Brillouin zone,

$$\mathbf{j}(t) = \sum_{mn} \int_{\text{BZ}} \frac{d\mathbf{k}}{(2\pi)^3} \langle n\mathbf{k}_t | \partial_{\mathbf{k}_t} h(\mathbf{k}_t) | m\mathbf{k}_t \rangle \rho_{mn}(\mathbf{k}; t), \quad (3)$$

where the Hamiltonian gradient  $\partial_{\mathbf{k}_t} h(\mathbf{k}_t)$  is obtained from the tight-binding model in an analytic form, and its matrix element in the above formula represents the operator observable corresponding to the total current density (for simplicity, we do not decompose  $\mathbf{j}(t)$  into intra- and inter-band currents).

An important aspect of the method is the grid of  $\mathbf{k}$ -vectors sampling the Brillouin zone, which must be sufficiently dense for the integral (3) to converge. The convergence properties with respect to the Brillouin-zone

sampling density were discussed in detail in [27]. For this work, we sample the reciprocal-space cell with an equidistant grid of  $128^3$  grid points. The grid is aligned with the reciprocal basis vectors and it is invariant under the symmetry operations of the material.

#### IV. SIMULATION RESULTS

##### A. Response from a portion of the Brillouin zone

For a crystalline sample with a fixed orientation, we assume a linearly polarized optical pulse driving the current-density response, which is subsequently converted into a spectrum. For a given  $\mathbf{k}$ , the integrand in (3) represents the contribution of this  $\mathbf{k}$ -spot inside the Brillouin zone to the total response. Because it is often assumed that  $\mathbf{k}$  from a close vicinity of  $\Gamma$  contribute most to the HHG spectrum, we define a partially-sampled current density as

$$\mathbf{j}(r, t) = \sum_{\text{BZ}, |\mathbf{k}| < r} \int \frac{d\mathbf{k}}{(2\pi)^3} \langle n\mathbf{k}_t | \partial_{\mathbf{k}_t} h(\mathbf{k}_t) | m\mathbf{k}_t \rangle \rho_{mn}(\mathbf{k}; t). \quad (4)$$

In other words, for a given “radius”  $r$  we only include the current-density contributions from the initial  $\mathbf{k}$ -vectors that are closer to  $\Gamma$  than  $r$ . The central question in what follows is how large  $r$  one must take for  $\mathbf{j}(r, t)$  to be an accurate approximation of the total current density  $\mathbf{j}(t)$ .

##### B. HHG from a vicinity of the $\Gamma$ -point

Motivated by the assumption that high-harmonic radiation is mostly mediated by the electronic states close to the  $\Gamma$ -point of the Brillouin zone, we first look at the spectra generated by such states. We select a portion of the zone with a radius of  $r = 1$  (in units of inverse lattice constant), and calculate their collective contribution to  $\mathbf{j}(r = 1, t)$  and then the corresponding HHG-spectrum. During this and the following simulations, we make sure that all symmetry-related  $\mathbf{k}$ -points are simultaneously included, so that the calculated response has the correct material symmetry. This particular (i.e. for  $r = 1$ ) symmetry-respecting “ $\Gamma$ -vicinity” contains only about 0.4% of the total Brillouin-zone volume, so it is rather small.

As a first example, take GaAs excited by a  $3.5\mu\text{m}$  pulse with the electric-field amplitude of  $8.7\text{MV}/\text{cm}$ , polarized along the  $[011]$  direction. For this sample orientation, one expects the odd harmonics to be  $p$ -polarized, i.e. parallel to the excitation, while the even harmonics should be  $s$ -polarized.

Figure 1 shows the simulated HHG-spectra, generated by the electronic states that are initially in the  $\Gamma$ -vicinity, compared to the spectrum in which the entirety of the Brillouin zone was included. For the  $p$ -polarization, the two HHG-spectra are quite similar. Keeping in mind

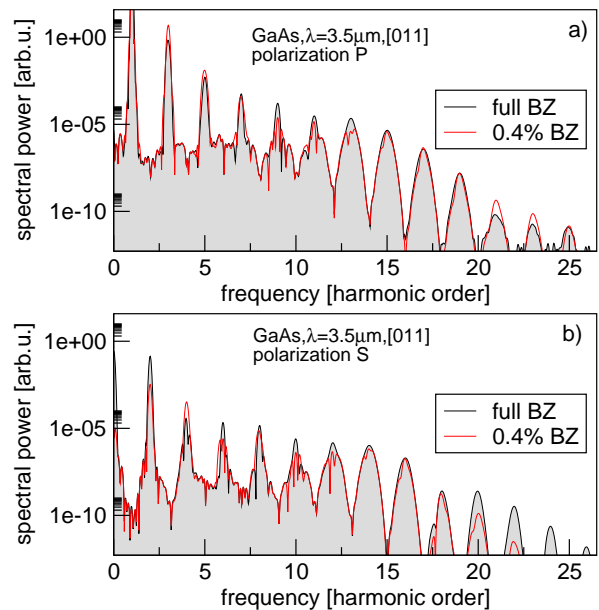


FIG. 1. GaAs high-harmonic spectrum from the full Brillouin zone (black, gray-filled line) compared to that generated from a vicinity of  $\Gamma$ -point encompassing 0.4% of the total Brillouin-zone volume (red line), for a) parallel and b) perpendicular polarization. The excitation pulse, at  $\lambda = 3.5\mu\text{m}$  wavelength, is polarized along  $y = z$  direction.

that the scale of the figure is logarithmic, one can see that the largest deviations between the two spectra are about one order of magnitude or only slightly larger. For the  $s$ -polarized response, the gap between the partial and total spectra opens a bit more, especially for the second harmonic and the harmonics above the order of eighteen. Nevertheless, the fact that merely 0.4% of the Brillouin zone volume produces a HHG response so close to the total suggest that the  $\Gamma$ -point indeed dominates the HHG process as is often assumed in various semi-classical analyses.

This is an encouraging observation, but it would be premature to conclude that the prominence of the  $\Gamma$ -point as the HHG-source is a typical behavior. For the next example, the excitation wavelength is chosen twice as long,  $\lambda = 7\mu\text{m}$ . The expectation is, perhaps, that in response to longer wavelengths a small vicinity of the Brillouin-zone center also generates most of the harmonic power; Indeed, one could argue that a longer wavelength implies a more off-resonant tunneling excitation of electrons into the conduction bands, which should translate into carriers being “born” in a tighter neighborhood of  $\Gamma$ . As a result, even smaller portion of the Brillouin zone could be responsible for the harmonic response.

However, Fig. 2 shows otherwise. While all conditions with the exception of the excitation wavelength are exactly the same as in the former example, one can see a dramatic difference between the partial and full spectra. Perhaps one should consider a larger volume around the center of the zone, but in the light of the previous illus-

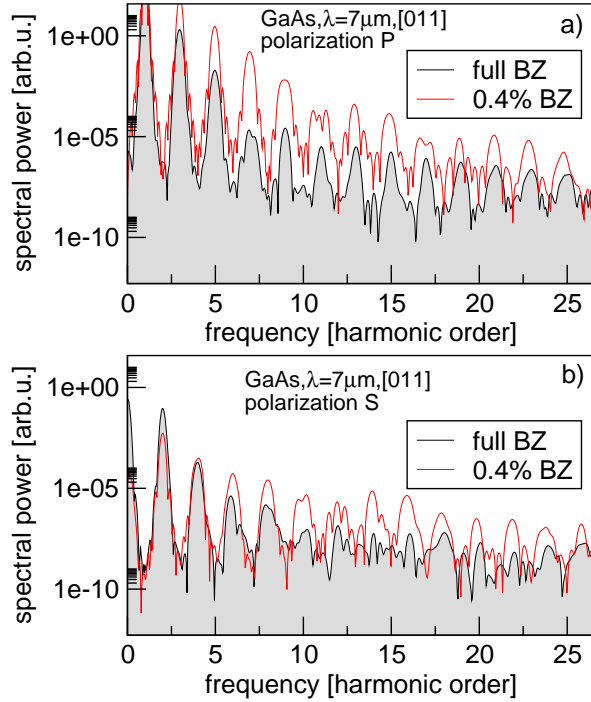


FIG. 2. GaAs high-harmonic spectrum from the full Brillouin zone (black, gray-filled line) compared to that generated from a vicinity of  $\Gamma$ -point encompassing 0.4% of the total Brillouin-zone volume (red line), for A) parallel and B) perpendicular polarization. The excitation pulse, at  $\lambda = 7\mu\text{m}$  wavelength, is polarized along  $y = z$  direction.

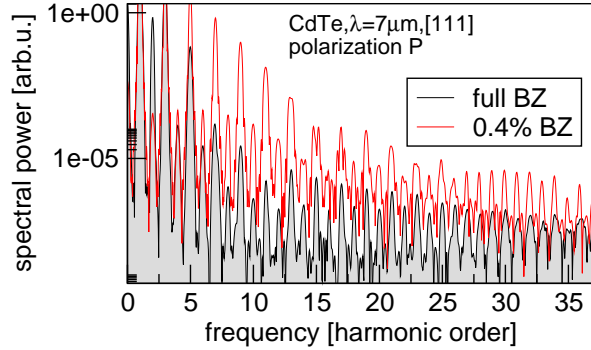


FIG. 3. CdTe high-harmonic spectrum from the full Brillouin zone (black, gray-filled line) compared to that generated from a vicinity of  $\Gamma$ -point encompassing 0.4% of the total Brillouin-zone volume (red line). The excitation pulse, at  $\lambda = 7\mu\text{m}$  wavelength, is polarized along  $x = y = z$  direction.

tration, this result is rather surprising. Yet, it turns out that it is more typical...

Figure 3 shows an analogous comparison of partial and full-zone spectra for CdTe. A recent study showed that the high-harmonic generation is significantly stronger in this material, and the relatively flat conduction-band shape was identified as a possible reason. The higher density of states around  $\Gamma$  should further emphasize its

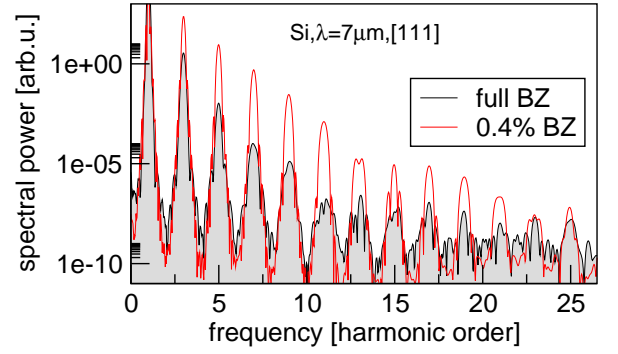


FIG. 4. Silicon high-harmonic spectrum from the full Brillouin zone (black, gray-filled line) compared to that generated from a vicinity of  $\Gamma$ -point encompassing 0.4% of the total Brillouin-zone volume (red line). The excitation pulse, at  $\lambda = 7\mu\text{m}$  wavelength, is polarized along  $x = y = z$  direction.

contribution to the response, and this is why the material was selected for our next example. Here we have chosen to change the excitation-pulse polarization to  $[111]$ , for which both even and odd harmonics appear in the  $p$ -polarization, while the  $s$ -polarized response vanishes. The figure shows a range of frequencies similar to that observed in the experiments [30]. In a qualitative agreement with the experiment, a rather strong set of harmonics forms between order 20 and 30, and their relative powers appear to be in the right ballpark. We therefore trust that this simulation, too, is sufficiently realistic. The important takeaway from this numerical experiment is that the small central portion of the Brillouin zone provides a poor approximation of the actual HHG spectrum. While the qualitative “shape” and relative peak powers are qualitatively very similar between the two spectra, the partial response is orders of magnitude *stronger*.

As yet another example, we choose crystalline Silicon as an inversion-symmetric material with an indirect band-gap. The sample orientation and the properties of the excitation pulse are the same as in the previous case, i.e.  $\lambda = 7\mu\text{m}$  and the electric field oscillation direction is  $[1,1,1]$ . Figure 4 shows, once again, that the immediate neighborhood of  $\Gamma$  does not produce a HHG response which could be compared to that from the full Brillouin zone. One could even argue that the difference here is larger than that in the previous examples. Indeed, the harmonic orders 7 — 11 appear to be four to five orders of magnitude stronger than those generated from the full Brillouin zone. We speculate that this could be the manifestation of the indirect gap of this material.

To summarize this subsection, we have shown that the high-harmonic spectra generated from a small neighborhood of the Brillouin zone center are not, at least not in general, good approximation of the full response. Thus, one needs to go beyond the immediate vicinity of the  $\Gamma$ -point to obtain a more precise representation of the HHG-spectra. In the following subsection we quantify how large the integration region should be.



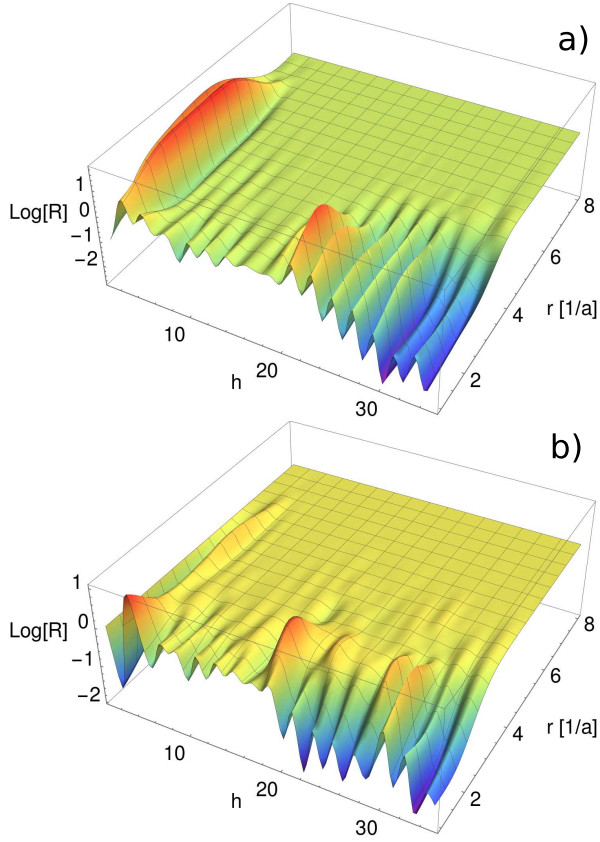


FIG. 5. Convergence of the simulated spectrum for GaAs excited along [011] at  $\lambda = 3.5\mu\text{m}$  (as in Fig. 1). Quantity  $\log[R(r, h)]$  (see text for details), representing the ratio of the partial ( $r < 7.025\dots$ ) to full-zone spectral power integrated over the harmonic band  $h$  is shown on a log scale. Top (a) and bottom (b) panels represent the results for the  $p$ - and  $s$ -polarized HHG spectra, respectively.

### C. Mapping the HHG-sources

In order to map the strength of the HHG source across the Brillouin zone, we set up a series of simulations for each of the studied materials. We increase the radius  $r$  of the  $\Gamma$ -centered subset of the Brillouin zone in steps of  $1a^{-1}$ , calculating the current-density  $\mathbf{j}(r, t)$  and the corresponding spectrum  $S(r, \omega)$  at each step, until the entirety of the zone is included. Note that the values  $r = \{1, 2, 3, 4, 5, 6, 7\}a^{-1}$  represent, respectively, 0.4, 3.4, 11, 27, 54, 86, and 99.99 percent of the full-zone volume. The goal of this mapping is to identify how large a portion of the Brillouin zone must be included for a reasonably accurate HHG simulation.

For the sake of visualization, the integrated harmonic-band power  $P(r, h)$  is calculated from the simulated spectrum  $S(r, \omega)$  in the given simulation as  $P(r, h) = \int_{(h-0.5)\omega_0}^{(h+0.5)\omega_0} |S(r, \omega)|^2 d\omega$ . The integration interval is always centered on the integer multiple of the fundamental frequency  $\omega_0$ , whether that particular harmonics is allowed by symmetry or not, and the interval is one

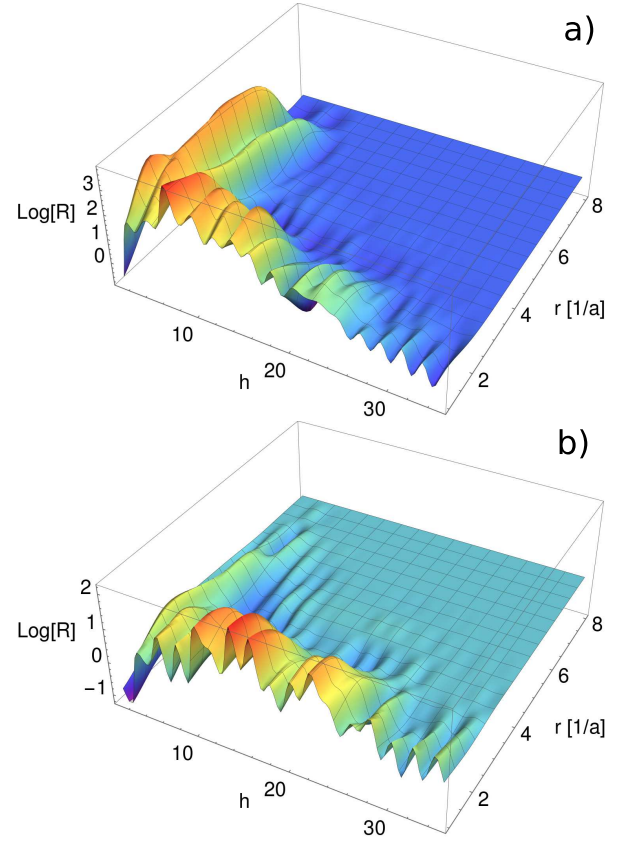


FIG. 6. Simulated spectrum convergence for GaAs excited along [011] at  $\lambda = 7\mu\text{m}$  (as in Fig. 2). a)  $p$ -polarized response, and b)  $s$ -polarized response.

harmonic order wide. The two-dimensional maps of  $R(r, h) = P(r, h)/P(r = 8, h)$  are plotted versus the order  $h$  and  $r \in (1, 8)a^{-1}$ . This quantity or, more precisely, its approach to unity, reflects the spectrum convergence since for  $r = 8$  the entire Brillouin zone is already included in the integration. (Note that  $r \approx 7.025$ , corresponding to  $|\Gamma W|$ , represents the entire zone.) To make the resulting graphs easier to interpret, at least for their global features, the interpolation order of the plot routine was set equal to three (resulting in an artificially smooth plotted surface). Since the log-scale is natural for simulated spectra,  $\log[R(r, h)]$  is depicted in the following two figures.

Figure 5 illustrates the convergence of the simulated spectrum with the increasing radius  $r$  of the portion of the Brillouin zone included in the simulation. The material here is GaAs and all conditions as for Fig. 1. Thus, this figure shows how the red curves in Fig. 1 gradually approach (with the increasing  $r$ ) the black curves corresponding to the full-zone spectrum.

Several features become evident; First, the below-gap harmonics are never accurate until  $r \approx 7a^{-1}$ , i.e. essentially until the entire zone is included in the simulation. Second, for the higher-order harmonics it takes  $r \approx 4a^{-1}$ , i.e. about 25% of the full-zone volume to obtain accurate

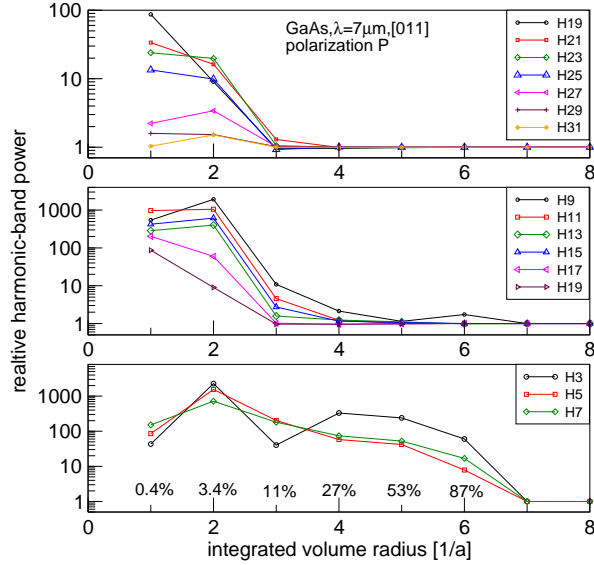


FIG. 7. Convergence of the  $p$ -polarized HHG spectrum for GaAs excited by a pulse polarized along  $y = z$  at  $\lambda = 7\mu\text{m}$ . Shown is the ratio  $R(r, h)$  between the spectral power (integrated over a harmonic band) obtained from a portion of the Brillouin zone and the corresponding power for the entire zone. Lines connecting the symbols only serve as a guide for the eye. Percentages shown in the lower panel represent the volume-portion of the whole zone.

simulated spectrum. Third, while quantitatively different, the convergence behaviors of the  $p$ - and  $s$ -polarized responses are similar.

Figure 6 shows similar results for the longer excitation wavelength,  $\lambda = 7\mu\text{m}$ , and corresponds to the transition between the extreme cases depicted in Fig. 2. Comparison to Fig. 5 shows that while the small- $r$  results are an order of magnitude less accurate (note the different vertical scale in the two figures), a good convergence (but for higher-order harmonic only) is achieved at about the same rate, and perhaps even faster at the high-frequency end of the spectrum. We note that the convergence behavior is very similar also in the cases of Silicon and CdTe, illustrated in Figures 3 and 4, and therefore their convergence-maps are not shown here.

For a more quantitative representation of the convergence of the simulated spectra as functions of the portion of the Brillouin zone included, Figs. 7 and 8 show the ratio  $R(r, h) = P(r, h)/P(r = 8, h)$  between the partial-spectrum and full-spectrum power integrated over the given harmonic band. The bottom panels show that the lower-order harmonics can not be obtained accurately unless the entire zone is integrated. The medium-high harmonic orders (shown in the middle panels) converge faster, with the partial-zone results accurate within an order of magnitude once the integrated zone-portion is larger than about one third. The high-order harmonics (top panels) become quite accurate already at about 25 to 50 percent of the entire zone included.

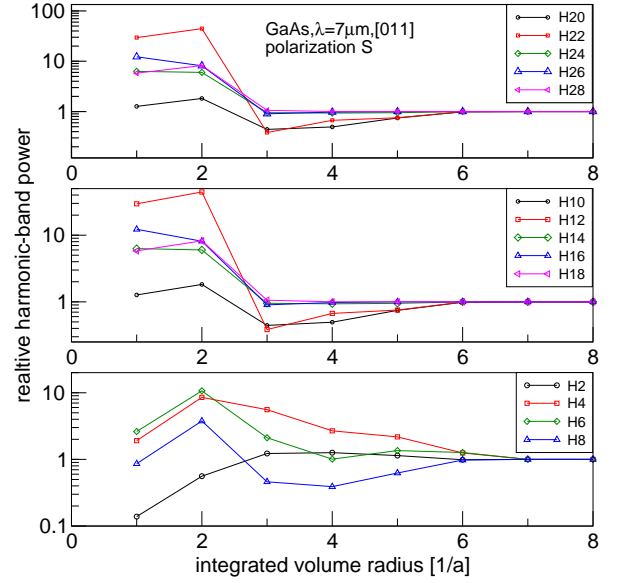


FIG. 8. Convergence of the  $s$ -polarized HHG spectrum for the same conditions as in Fig. 7.

So, to answer the question about the size of the zone that needs to be included in the simulation, it is hundred and roughly fifty percent for the below-gap and the above-gap harmonics, respectively. From the simulation standpoint, a fifty-percent increase in speed is probably not worth of the trouble...

On the other hand, this result is important for the interpretations of HHG dynamics in those cases where any kind of trajectory comes into consideration. It indicates that the starting points of the contributing trajectories should “cover” at least thirty to fifty percent of the Brillouin-zone volume, and that the corresponding contributions should be coherently added up to represent the total response of the material.

#### D. Mapping the tunneling rate

The finding that the Brillouin zone center in general does not contribute the most of the HHG response seems to contradict the highest tunneling probability in this region. Indeed, if the valence-to-conduction band excitation does behave as the tunneling ionization in atoms, then the rate of excitation should be exponentially sensitive to the  $k$ -dependent bandgap, and therefore fall-off quickly upon departure from the zone center. Based on this argument, one sometimes assumes that the carriers are only created *at* the point of the minimal gap.

The explanation is actually very simple. It turns out that the difference between the tunneling rates is counteracted by the fact that the volume of the Brillouin zone overshadows the vicinity of the  $\Gamma$  point. To illustrate this, we have measured the total population in all conduction bands combined. Figure 9 shows the result for

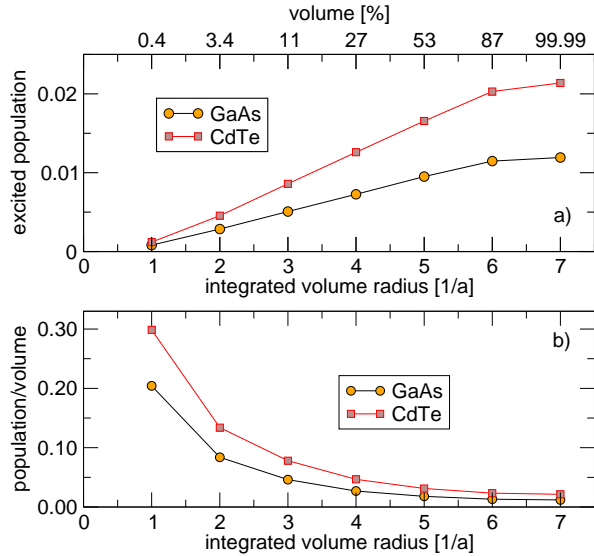


FIG. 9. Total population fraction of excited states inside the reciprocal-space integration volume centered on the  $\Gamma$ -point (a). The top horizontal axis shows the size of the volume as a percent-fraction of the full Brillouin zone. The lower panel, (b) shows the population divided by the volume which gives the average tunneling rate for the states inside the volume of radius  $r$ . As expected, the tunneling rate peaks in the center of the zone.

the examples of GaAs and CdTe excited with a  $\lambda = 7\mu\text{m}$  pulse. The top panel makes a case for the great majority of carriers being generated away from the  $\Gamma$  point. The lower panel depicts the total excited population in the integrated subset of the Brillouin zone divided by the volume of latter. As such it is a measure of the (averaged) tunneling rate. This quantity indeed shows that the excitation rate is greatly larger around the zone-center, precisely as expected. It is just that the contrast is not large enough to compensate for the much bigger volume of the peripheral regions of the Brillouin zone.

### E. The relevant energy bands

One sometimes makes an argument that a HHG spectrum, or perhaps just one of its peaks is generated by the contributions from a limited number of electronic bands, possibly from only a single valence-conduction pair. Indeed, this kind of an assumption underlines a number of approaches for all-optical reconstruction applied to the band-structures or to the  $k$ -dependent dipole moments.

To test which electronic bands give relevant contributions in the materials studied here, we have repeated the simulation with restricted sets of states. The restriction is realized by projecting the density matrix (or equivalently, by projecting the  $k$ -dependent Hamiltonian  $h(\mathbf{k})$ ) onto a subspace spanned by the select bands at each integration step.

The results will be illustrated on the case of GaAs, ex-

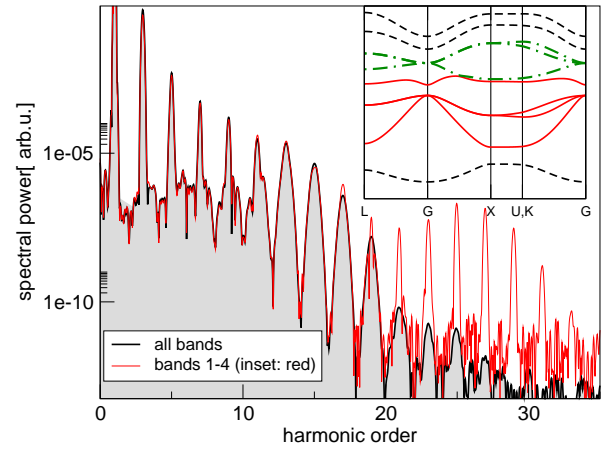


FIG. 10. High-harmonic spectrum from a reduced model. The black-line, shaded-area shows the spectrum obtained from the full simulation. The thin red line represents the result of a simulation restricted to the bands shown in full red lines in the inset.

cited with a  $\lambda = 3.5\mu\text{m}$  pulse (the situation corresponding to that illustrated in Fig. 1), but the observations are similar in all situations investigated in this work.

First, we select the bands 1 through 4 (labeling the lowest-energy band as 0). This selection accounts for the three highest valence bands and the lowest-energy conduction band. It seems reasonable to expect that these are the most important bands above and below the gap. We compare the resulting HHG spectrum to that obtained from the full simulation in Fig. 10 for the  $p$ -polarized component of the response. It is encouraging that the spectra are quite close to each other for harmonics lower than nineteen. However, one can see pronounced artifacts at the high-frequency end of the spectrum, where strong harmonic peaks appear which do not exist or which are about five orders of magnitude weaker in the full spectrum.

So if we ask which bands need to be included such that the corresponding spectrum is accurate across all frequencies, the set of one to four appears to be inadequate. We speculate that the reason is that the conduction band four makes a close approach to the group of higher-energy bands shown by dashed-dotted line in the inset of Fig. 10. In a time-dependent external field they become coupled and the populations and polarizations resulting from this coupling affect the dynamics.

Inclusion of the next conduction band does not improve the situation (data not shown); the artifacts at the higher-frequency side of the spectrum actually become slightly worse. Only after including the whole group five to seven (dark green dashed-dotted lines in Fig. 10) we obtain a HHG spectrum that is very close to the full spectrum with the exception of small deviations for the lowest-order harmonics.

So we come to the conclusion that while an individual harmonic peak could be approximated with a limited set

of electronic bands, to guarantee the accuracy for all harmonics, one should include all “energetically connected” bands below and above the bandgap.

## V. CONCLUSION

Numerical simulations of the high-harmonic generation in zinc blende materials GaAs and CdTe, and in crystalline Silicon were executed for two different excitation wavelengths while gradually including the nonlinear-response contributions from larger and larger portions of the Brillouin zone. The goal of this work was to determine how large is the region in the Brillouin zone that must be accounted for in a numerical simulation in order to produce quantitatively accurate spectra. It turns out that there is no simple answer to the question posed in the title of this work. Nevertheless, our comparative simulations offer useful insights into certain trends and behaviors which seem quite universal.

The assumption that the Brillouin zone center dominates the high-harmonic processes has been used in a number of HHG-interpretations, especially those incorporating aspects of the semi-classical approaches. However, we have found that this assumption is not justified, at least not in general. While we have identified an example where the  $\Gamma$ -neighborhood encompassing merely 0.4 percent of the Brillouin zone volume does provide a HHG spectrum accurate within one order of magnitude globally and with a much better accuracy locally (specifically for the medium-order harmonic orders), we have also found several cases where the contribution from the zone center is orders of magnitude different from the total spectrum. Interestingly, in such cases the central contribution appears to be *stronger* than that of the whole zone, and this indicates that destructive interferences occur across the Brillouin zone.

On the other hand, it turns out that for (only) the above-the-gap frequencies, the center of the zone produced *qualitatively correct* spectra in all cases studied in this work. The zone-center HHG spectra exhibited stronger peak-to-valley contrast, but the overall spectrum shapes were good. We therefore think that, in the light of these results, the approximations restricted to the  $\Gamma$  point (or to a small vicinity of it) remain justified for *qualitative* investigations into underlying physics. However, it should be emphasized that no matter how small a portion of the Brillouin zone is used, the sampling grid must have the symmetry of the material.

For the simulations which aim for a higher accuracy, we conclude that a significant portion of the Brillouin zone must be integrated over. Of course, precisely how large it should be depends on the expected accuracy, material, and the excitation wavelength. As a rough estimate, thirty to fifty percent of the zone volume should be included for a simulated spectrum with the harmonic peaks accurate within an order of magnitude or better. In terms of the excitation wavelength, we observed that while the

spectra generated from the zone center were more accurate for the shorter wavelength, the convergence toward the full-zone solution seems somewhat faster for the longer wavelength, i.e. a smaller part of the Brillouin zone can suffice. We speculate that this is because the carriers are driven further across the Brillouin zone in the latter case.

We trust that these observations will prove useful for a number of applications concerning solid-state high-harmonic generation, including all-optical band-structure reconstruction and/or optical measurements of Berry curvatures and shift vectors. Analyses which rely on the assumption of specific starting points for the relevant trajectories, could be generalized to account for the fact that in reality a “distribution of,” or a bundle of trajectories should provide a physically more realistic picture.

Another finding with potential impact on such applications is that care should be exercised when one wants to restrict the number of electronic bands believed to account for the relevant response contributions. We have found that in order to obtain good accuracy across all frequencies, all bands that are connected or that closely approach each other somewhere in the Brillouin zone must be included. In other words, it should be safer to apply various reconstruction algorithms to the whole “connected groups” of electronic bands.

A rather surprising outcome of this study is that the lower-order, below-the-gap harmonics always require the integration of all response-contributions across the entirety of the Brillouin zone. This finding is important for the future microscopic-level modeling of laser materials, such as zinc-blende wide gap semiconductors. Whenever the nonlinear propagation of optical pulses plays a role, the second- and third-harmonic responses in particular must be sufficiently accurate. This work shows that the Brillouin zone center alone is insufficient to yield accurate description for the nonlinear properties at frequencies below the gap.

Our work concentrated on the three-dimensional materials, and it is not a given that the results apply to the (effectively) two-dimensional systems, where the central part of the Brillouin zone constitutes a much larger fraction of its volume. On one hand, one could argue that such an investigation is less important from the practical standpoint, because even complete sampling of two-dimensional Brillouin zones does not present any significant numerical challenge. On the other hand, it will be interesting to extend the present study to two-dimensional materials for the conceptual reasons, for example to improve the semi-classical interpretations.

## ACKNOWLEDGMENTS

Authors acknowledge the support from the Air Force Office for Scientific Research under grants no. FA9550-22-1-0182 and FA9550-21-1-0463.



- 
- [1] S. Ghimire, A. D. DiChiara, E. Sistrunk, P. Agostini, L. F. DiMauro, and D. A. Reis, Observation of high-order harmonic generation in a bulk crystal, *Nature Physics* **7**, 138 (2011).
  - [2] J. Park, A. Subramani, S. Kim, and M. F. Ciappina, Recent trends in high-order harmonic generation in solids, *Advances in Physics: X* **7**, 2003244 (2022).
  - [3] S. Ghimire and D. A. Reis, High-harmonic generation from solids, *Nature Physics* **15**, 10 (2019).
  - [4] E. Goulielmakis and T. Brabec, High harmonic generation in condensed matter, *Nature Photonics* **16**, 411 (2022).
  - [5] G. Vampa, T. J. Hammond, N. Thiré, B. E. Schmidt, F. Légaré, C. R. McDonald, T. Brabec, D. D. Klug, and P. B. Corkum, All-optical reconstruction of crystal band structure, *Phys. Rev. Lett.* **115**, 193603 (2015).
  - [6] A. A. Lanin, E. A. Stepanov, A. B. Fedotov, and A. M. Zheltikov, Mapping the electron band structure by intraband high-harmonic generation in solids, *Optica* **4**, 516 (2017).
  - [7] A. J. Uzan-Narovlansky, A. Jiménez-Galán, G. Orenstein, R. E. F. Silva, T. Arusi-Parpar, S. Shames, B. D. Bruner, B. Yan, O. Smirnova, M. Ivanov, and N. Dudovich, Observation of light-driven band structure via multiband high-harmonic spectroscopy, *Nature Photonics* **16**, 428 (2022).
  - [8] Y. Qiao, Y.-Q. Huo, S.-C. Jiang, Y.-J. Yang, and J.-G. Chen, All-optical reconstruction of three-band transition dipole moments by the crystal harmonic spectrum from a two-color laser pulse, *Opt. Express* **30**, 9971 (2022).
  - [9] D. Wu, L. Li, Y. Zhan, T. Huang, H. Cui, J. Li, P. Lan, and P. Lu, Determination of transition dipole moments of solids with high-order harmonics driven by multicycle ultrashort pulses, *Phys. Rev. A* **105**, 063101 (2022).
  - [10] S. Jiang, H. Wei, J. Chen, C. Yu, R. Lu, and C. D. Lin, Effect of transition dipole phase on high-order-harmonic generation in solid materials, *Phys. Rev. A* **96**, 053850 (2017).
  - [11] S. Jiang, J. Chen, H. Wei, C. Yu, R. Lu, and C. D. Lin, Role of the transition dipole amplitude and phase on the generation of odd and even high-order harmonics in crystals, *Phys. Rev. Lett.* **120**, 253201 (2018).
  - [12] Y. Qiao, Y. Huo, H. Liang, J. Chen, W. Liu, Y. Yang, and S. Jiang, Robust retrieval method of crystal transition dipole moments by high-order harmonic spectrum, *Phys. Rev. B* **107**, 075201 (2023).
  - [13] D. Baykusheva, A. Chacón, J. Lu, T. P. Bailey, J. A. Sobota, H. Soifer, P. S. Kirchmann, C. Rotundu, C. Uher, T. F. Heinz, D. A. Reis, and S. Ghimire, All-optical probe of three-dimensional topological insulators based on high-harmonic generation by circularly polarized laser fields, *Nano Letters* **21**, 8970 (2021).
  - [14] A. J. Uzan, G. Orenstein, A. Jiménez-Galán, C. McDonald, R. E. F. Silva, B. D. Bruner, N. D. Klimkin, V. Blanchet, T. Arusi-Parpar, M. Krüger, A. N. Rubtsov, O. Smirnova, M. Ivanov, B. Yan, T. Brabec, and N. Dudovich, Attosecond spectral singularities in solid-state high-harmonic generation, *Nature Photonics* **14**, 183 (2020).
  - [15] G. Bae, Y. Kim, and J. D. Lee, Revealing Berry curvature of the unoccupied band in high harmonic generation, *Phys. Rev. B* **106**, 205422 (2022).
  - [16] C. P. Schmid, L. Weigl, P. Grössing, V. Junk, C. Gorini, S. Schlauderer, S. Ito, M. Meierhofer, N. Hofmann, D. Afanasiev, J. Crewse, K. A. Kokh, O. E. Tereshchenko, J. Gädde, F. Evers, J. Wilhelm, K. Richter, U. Höfer, and R. Huber, Tunable non-integer high-harmonic generation in a topological insulator, *Nature* **593**, 385 (2021).
  - [17] G. Vampa, C. R. McDonald, G. Orlando, P. B. Corkum, and T. Brabec, Semiclassical analysis of high harmonic generation in bulk crystals, *Phys. Rev. B* **91**, 064302 (2015).
  - [18] G. Vampa and T. Brabec, Merge of high harmonic generation from gases and solids and its implications for attosecond science, *Journal of Physics B: Atomic, Molecular and Optical Physics* **50**, 083001 (2017).
  - [19] L. Yue and M. B. Gaarde, Introduction to theory of high-harmonic generation in solids: tutorial, *J. Opt. Soc. Am. B* **39**, 535 (2022).
  - [20] D. Tang and X.-B. Bian, Multiple collisions in crystal high-order harmonic generation, *Chinese Physics B* **31**, 123202 (2022).
  - [21] L. Li, P. Lan, X. Zhu, T. Huang, Q. Zhang, M. Lein, and P. Lu, Reciprocal-space-trajectory perspective on high-harmonic generation in solids, *Phys. Rev. Lett.* **122**, 193901 (2019).
  - [22] L. Li, P. Lan, X. Zhu, and P. Lu, Huygens-fresnel picture for high harmonic generation in solids, *Phys. Rev. Lett.* **127**, 223201 (2021).
  - [23] T. Huang, L. Li, J. Li, X. Zhu, P. Lan, and P. Lu, Polarization-resolved analysis to solid high-order harmonic generation, *Journal of Physics B: Atomic, Molecular and Optical Physics* **55**, 093001 (2022).
  - [24] L. Yue and M. B. Gaarde, Expanded view of electron-hole recollisions in solid-state high-order harmonic generation: Full-Brillouin-zone tunneling and imperfect recollisions, *Phys. Rev. A* **103**, 063105 (2021).
  - [25] P. Xia, T. Tamaya, C. Kim, F. Lu, T. Kanai, N. Ishii, J. Itatani, H. Akiyama, and T. Kato, High-harmonic generation in GaAs beyond the perturbative regime, *Phys. Rev. B* **104**, L121202 (2021).
  - [26] P. Xia, C. Kim, F. Lu, T. Kanai, H. Akiyama, J. Itatani, and N. Ishii, Nonlinear propagation effects in high harmonic generation in reflection and transmission from gallium arsenide, *Opt. Express* **26**, 29393 (2018).
  - [27] M. Kolesik, Continuum limit and dephasing in the off-resonant strong-field interactions in solids, *Physical Review B* (submitted).
  - [28] M. Kolesik, Assessment of tight-binding models for high-harmonic generation in zinc blende materials, *Opt. Lett.* **48**, 3191 (2023).
  - [29] J. Gu and M. Kolesik, Full-Brillouin-zone calculation of high-order harmonic generation from solid-state media, *Phys. Rev. A* **106**, 063516 (2022).
  - [30] Z. Long, H. Yang, K. Tian, L. He, R. Qin, Z.-Y. Chen, Q. J. Wang, and H. Liang, High-harmonic generation in CdTe with ultra-low pump intensity and high photon flux, *Communications Physics* **6**, 228 (2023).
  - [31] P. Vogl, H. P. Hjalmarson, and J. D. Dow, A semi-empirical tight-binding theory of the electronic structure of semiconductors†,

- Journal of Physics and Chemistry of Solids **44**, 365 (1983).
- [32] A. D. Carlo, Microscopic theory of nanostructured semiconductor devices: beyond the envelope-function approximation, Semiconductor Science and Technology **18**, R1 (2002).
- [33] M. Fornari, H. H. Chen, L. Fu, R. D. Graft, D. J. Lohrmann, S. Moroni, G. P. Parravicini, L. Resca, and M. A. Strosio, Electronic structure and wave functions of interface states in HgTe-CdTe quantum wells and superlattices, Phys. Rev. B **55**, 16339 (1997).